SIMULATIONS OF HYDROGEN DISPERSION FROM FUEL CELL VEHICLES' LEAKAGES INSIDE FULL-SCALE TUNNEL

Koutsourakis, N.[1], Giannissi, S.G.[1], Tolias, I.C.[1], Venetsanos, A.G.[1], Forero, D.[2], Studer, E.[2]
[1] Environmental Research Laboratory, National Centre for Scientific Research "Demokritos", Agia Paraskevi, Athens, 15341, Greece, nk@ipta.demokritos.gr
[2] Univ. Paris-Saclay, CEA, Service de Thermohydraulique et de Mécanique des Fluides, F-91191 Gif-sur-Yvette, France

ABSTRACT

In this work, real scale experiments involving hydrogen dispersion inside a road tunnel have been modelled using the Computational Fluid Dynamics (CFD) methodology. The aim is to assess the performance of the ADREA-HF CFD tool against full-scale tunnel dispersion data resulting from high-pressure hydrogen leakage through Thermal Pressure Relief Device (TPRD) of a vehicle. The assessment was performed with the help of experiments conducted by the French Alternative Energies and Atomic Energy Commission (CEA) in a real inclined tunnel in France. In the experiments, helium as hydrogen surrogate has been released from 200 bar storage pressure. Several tests were carried out examining different TPRD sizes and release directions (upwards and downwards). For the CFD evaluation two tests were considered: one with downwards and one with upwards release, both through a TPRD with a diameter of 2 mm. The comparison between the CFD results and the experiments shows the good predictive capabilities of the ADREA-HF code that can be used as a safety tool in hydrogen dispersion studies. The comparison reveals some of the strengths and weaknesses of both the CFD and the experiments. It is made clear that CFD can contribute to the design of the experiments and to the interpretation of the experimental results.

1.0 INTRODUCTION

1.1 Motivation

The expected broad use of hydrogen as an energy carrier in the near future [1] will probably make its utilization in zero-emissions' fuel cell vehicles inevitable, especially in cases where fast refuelling and high autonomy are necessary. In 2021, there were already about 51600 hydrogen vehicles in the world [2]. The buoyancy of hydrogen makes it relatively safe to use in the open road, but in confined spaces like tunnels, security concerns arise due to its high flammability. The HyTunnel-CS EU-funded project (Pre-normative research for safety of hydrogen driven vehicles and transport through tunnels and similar confined spaces) focused on hydrogen safety within tunnels. During the project the release, dispersion and explosion of hydrogen inside road tunnels and other confined spaces was studied experimentally and numerically, with the aim of understanding the underlying physical phenomena and providing recommendations for regulations, codes and standards.

One of the objectives of the HyTunnel-CS project was to perform experiments of hydrogen dispersion at both reduced and full scale tunnels, since such experiments were not available at the literature. Part of the reduced-scale experiments of the project is used in another paper of the current conference as a validation dataset in order to successfully assess the performance of the ADREA-HF CFD code regarding hydrogen dispersion in tunnels [3]. A question arises though about what the CFD performance would be against a more challenging case of a real, full-scale tunnel, in a much more uncontrollable physical environment. In the current work we compare the experimental measurements of helium dispersion in a full-scale tunnel at France, with those of the relevant results of ADREA-HF.

Another issue that motivated this work is the fact that in the framework of the HyTunnel-CS project, ADREA-HF was among others used as a tool to assess the influence of the tunnel slope on hydrogen dispersion, for both ventilated and non-ventilated cases. Part of that work was presented at the previous IHCS conference [4]. The use of the particular code was justified since it has been extensively validated against hydrogen dispersion cases [5]. No comparison with experimental data of

hydrogen dispersion in inclined tunnels was performed though, since no such data were available by that time. The particular tunnel that is simulated in the current work partly resolves this issue, since it is sloped, with an inclination of 3.6%. Furthermore, at the two experimental tests that are chosen to be simulated, the in-tunnel wind is low and it acts against the buoyancy, which is the most unfavourable case of sloped tunnels and the most difficult to simulate [4,6]. Thus the current comparison of CFD results with the experimental measurements is both interesting and demanding.

1.2 Short review

One of the first CFD simulations of hydrogen dispersion from a vehicle was performed from Venetsanos et al. [7], who investigated an accident that happened in Stockholm at 1983 after the release of 13.5 kg of hydrogen from a delivery truck. That and many other similar studies since then revealed the usefulness and power of CFD in hydrogen safety assessment. Recently, Huang et al. [8] analysed with Large Eddy Simulation (LES) the hydrogen dispersion below a car and showed that hydrogen is transferred upwards intermittently from the back and sides of the car.

Regarding CFD simulations of hydrogen dispersion inside tunnels, one of the early studies was that of Middha and Hansen [9], who examined several scenarios including car and bus releases for various ventilation speeds. This and other relevant studies [10-14] have contributed in understanding the way hydrogen goes to the ceiling of the tunnel and propagates along it. Recent similar work can also be found at the HyTunnel-CS project (https://hytunnel.net/). Concerning sloped tunnels, most dispersion simulations are related to smoke and fires (see [4] for a short review), that are expected to present several similarities with hydrogen due to their buoyant nature. The work of Mukai et al. [11] is one of the first and few studies that deal with hydrogen dispersion in inclined tunnels. Contours of hydrogen propagation throughout the tunnel for the cases of longitudinally “V-shaped” and “Lambda-shaped” tunnels are presented. In the latter case hydrogen is trapped at the ceiling. The release rate of that study was very low though and of course no comparison with experimental data was provided.

2.0 DESCRIPTION OF THE EXPERIMENTS

In the framework of HyTunnel-CS, CEA has performed two experimental campaigns, at 2020 and 2021, in a real tunnel in France. Here only the dispersion experiments of 2020 are examined, for which the non-flammable helium was used as a hydrogen surrogate. This is a common practice when safety is demanded while investigating hydrogen dispersion [15]. Due to the strong buoyant nature of both elements, we can consider the conclusions from helium experiments similar to those of hydrogen ones.

The experiments were carried out in the Tunnel du Mortier, at an elevation of 1391 m, at Autrans ski resort, near Grenoble. This is a disused, 502 m long horseshoe-type straight road tunnel. The first 133 m from the Autrans side is concreted, while almost all the rest of the tunnel consists of rough rock. The measurements took place at the concrete section (Figure 1c), at 72 m from the entrance, where the tunnel is about 7.5 m wide and 5.1 m high. The slope is 3.6% (the Autrans entrance has higher elevation) and there is no mechanical ventilation. Two straw walls were installed at each end of the tunnel to limit natural convection.

The vehicle which represents the car consists actually of a horizontal plate 4.5 m long and 1.9 m wide. The front part of the vehicle is loaded with equipment, including the tank of about 50 litters at 200 bar. The discharge is performed from a TPRD located at 15 cm from the back end of the vehicle (Figure 1a). The TPRD can be oriented towards the ceiling (protruding from the car) or downwards. The vehicle is positioned centrally in the tunnel and its distance from the ground varies between about 21.5 cm along the street axis and over 23.5 cm at the sides of the vehicle (the road is unevenly curved).

The concentration measurements were performed with the use of eight vertical masts located between +/- 24 m around the injection point (Figure 1b), named from M1 to M8. Depending on the test case, additional laboratory supporting masts were also present (red at Figure 1b). Each mast carried many sensors measuring for example O_2, CO_2, temperature, humidity, but only the helium sensors will be

considered here. Those sensors were of thermal conductivity type, had a measuring uncertainty of 0.1% vol. and their typical response time was about 1 s. In the case of upwards releases, the helium sensors were 20, placed mainly close to the ceiling. For the downwards releases many sensors were repositioned around the car and two additional ones were added. The coordinates of the sensors are provided later, for the coordinate system of the simulations, which has the X-axis along the tunnel.

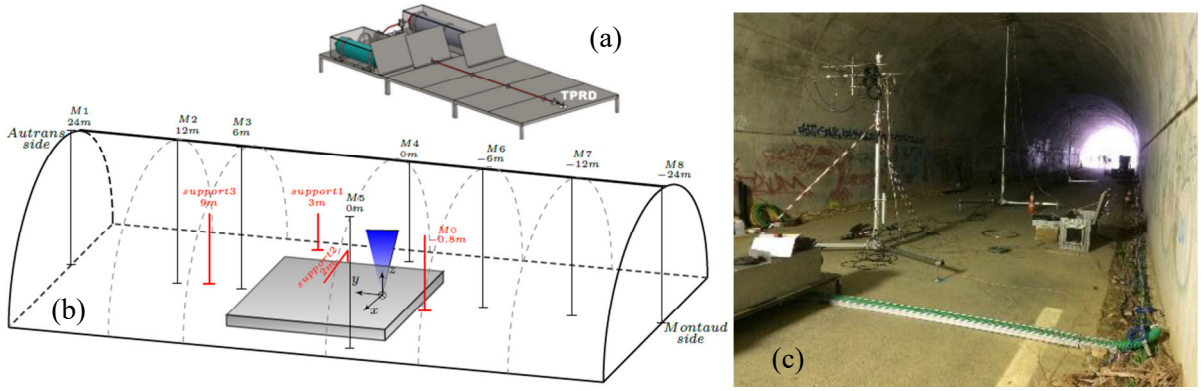

Figure 1. (a) The vehicle used. (b) A sketch of the part of the tunnel where the measurements were performed. (c) A photograph of part of the tunnel with some of the masts; the front part of the vehicle and the Autrans exit of the tunnel can be seen

The experimental campaign included a dozen of dispersion tests, with different release directions and TPRD diameters between 0.5 and 3 mm. For this work only tests "3" and "12" were considered, with a TPRD of 2 mm, which is a typical one. At test 12 the release is downwards, which is the common practice for fuel cell vehicles and at test 3 it is upwards, which also covers the case of the car being upside-down due to a hypothetical accident. The decreasing helium release mass flow rate (blowdown) can be estimated from experimental measurements at the tank. The blowdown time is considered to be 280 s for both tests of this work. In case of test 12 the TPRD pointed downwards through a hole on the chassis; that hole was closed around the TPRD during all the experiments.

The wind speed was monitored at only one point inside the tunnel (on top of support 3 - Figure 1b). At test 12 wind speed varied between -0.41 m/s and -0.65 m/s, with an average of -0.56 m/s during the first 500 seconds, while at test 3 the wind varied between -0.30 m/s and -0.51 m/s, with an average of -0.35 m/s during the first 200 seconds. Ambient temperature and pressure was about 6.5 ^{o}C, 0.861 bar and 8.5 ^{o}C, 0.854 bar for tests 12 and 3 respectively. More information about the experimental campaign and its measurements can be found at [16,17] and at HyTunnel-CS reports.

3.0 DESCRIPTION OF THE SIMULATIONS

For the simulations, the Reynolds Averaged Navier-Stokes (RANS) CFD methodology is used, as implemented in the ADREA-HF code, which employs the finite volume method on a staggered Cartesian grid. The basic 3D time-dependent conservation equations of the code are presented at [3]. The geometry is reproduced with the use of porosities, which makes possible the correct representation of any solid obstacle on any mesh [18], decoupling the geometry from the grid. The time step is adapted according to error bands and desired Courant– Friedrichs–Lewy (CFL) number.

ADREA-HF can be used at both incompressible and compressible flows. At the current cases, the helium release speed is equal to the speed of sound. This makes the simulation very demanding, especially in the case of downwards release, where there is a high-speed impinging jet, which is prone to numerical errors. Thus, for the discretization of the convective terms the high-order MUSCL numerical scheme [19] is used for all variables, which has been proven to provide good results in such cases [20,21]. For the turbulence closure the standard k-ε model is chosen, which is the most widely used. The ambient pressure and temperature as provided from the experimental measurements are applied and no energy equation is solved. Tunnel slope is modelled by changing the gravitational

direction in the momentum equations and by setting the appropriate initial hydrostatic pressure. Helium was chosen as second working fluid, from the gases library of ADREA-HF.

Based on on-site measurements, the geometry of the vehicle and of the tunnel is reproduced with minor simplifications at 'EDes', the geometrical pre-processor of ADREA-HF. The tunnel cross-section was considered constant for the simulations, with a total height of 5.12 m, a radius of 3.745 m (Figure 2) and an area of 32.33 m^2. The X-axis, along the tunnel, is positive towards the Autrans exit. X and Y axis' origins are at the TPRD, as in the experiment. Z-axis origin is at the ground level. A total length of 302 m was modelled, 72 m till the Autrans exit and the rest towards the other side. The computational domain was restricted to the tunnel itself, with no extension outside, which is usual for longitudinally ventilated tunnels. The bulk velocity was assumed to be the same with the value measured from the experiments (-0.56 m/s and -0.35 m/s for tests 12 and 3 respectively).

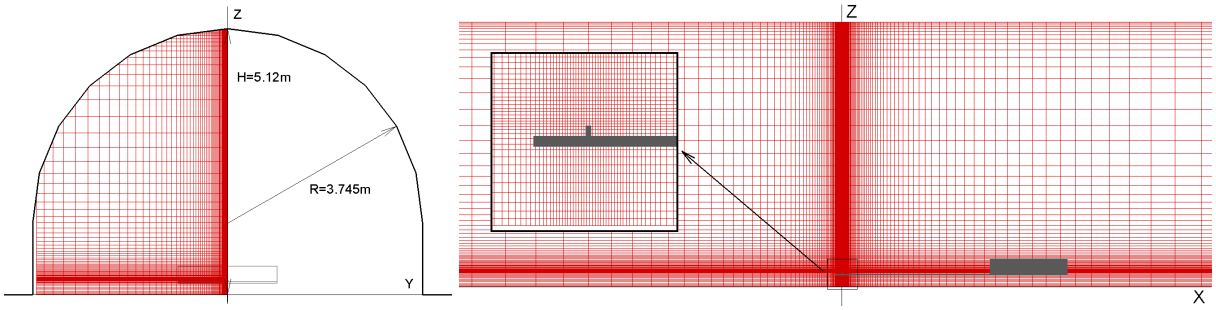

Figure 2. Part of the geometry and of the grid used for the simulations of test 3. At the inset the grid around the TPRD can be seen. The mesh shown represents the centres of the cells

In order to reduce the number of computational cells, a symmetry XZ plane at Y=0 was considered. The emitting surface was placed at the exit of the TPRD. Based on previous experience [4,20,21], four cells were used to discretize the release area. Due to symmetry, two of those cells were resolved. The grid around the release was uniform and then the cell size changed with a varying expansion ratio from 1.05 to 1.23. For higher simulation accuracy the grid was aligned with most important solid boundaries. The computational domain was 302 x 3.745 x 5.12 m^3, discretized as 192 x 58 x 76 cells in case of test 3 (Figure 2). In case of the downwards release, in order to better resolve the jet, the impingement and the recirculations below the car, the number of cells between the chassis and the ground was increased to 26 (instead of 10). Also at test 12, in order to account for the street curvature, an obstacle of 1 cm high and 1 m wide was added on the ground along the whole tunnel. The geometry configuration was such that the distance of the TPRD exit from the obstacle/street, was the same with that of the experiment. Another difference of the geometry of test 12 is that the 35 mm x 35 mm rectangular rods around the chassis were added below the car, since they are expected to play a role in the trapping of helium there, before it escapes upwards. The intermediate rectangular rods and the feet of the chassis are ignored though. It should be noted that for test 3 a finer grid was tested, with 227 cells in the X-axis instead of 192 and the differences were not significant.

At the simulations the Birch notional nozzle approach [22] was followed, in order to avoid solving the complex flow structure near the release point due to the under-expanded jet that is formed. A constant sonic velocity (about 986 m/s for test 3 and 982 m/s for test 12) was considered until the end of the release. At the simulations, as the mass flow decreased, the notional nozzle area also decreased; this way both the mass flow rate and the momentum were close to the experimental values, without changing the grid. The calculation of the initial notional nozzle area was based on the Birch84 [22] assumption that the jet expands to ambient pressure downstream of the nozzle having sonic velocity and ambient temperature. That initial area was 2.23 x 10^{-4} m^2, which is very close to the 2.25 x 10^{-4} m^2 surface at the exit face of the TPRD, to which the grid was aligned. It is noted that is acceptable to model the round jet as a rectangular one [21], since in practice both have similar behaviour. In Figure 3 the source mass flow rate as a function of time is provided for the experimental cases and for the CFD. At the simulations the blowdown is smoothed out and is the same for both tests.

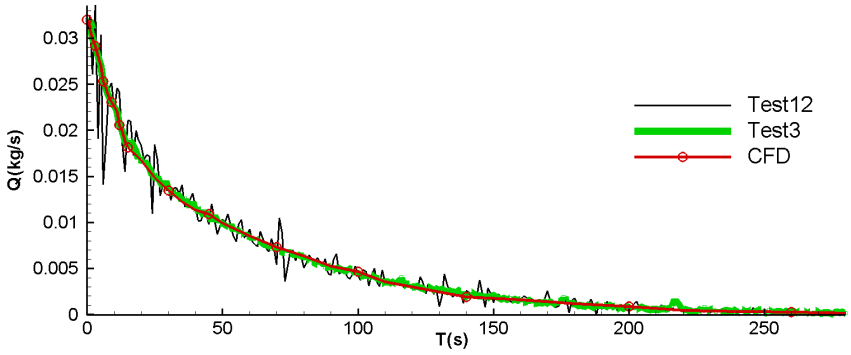

Figure 3. The TPRD mass flow rate of helium for the two experiments considered and the smoothed curve used for the simulations

At each of the cases examined a simulation without release was first performed, in order to establish the velocity field due to the wind. At the tunnel entrance, a uniform velocity parallel to the ground was considered, while at the exit, pressure outlet was applied. For the turbulent kinetic energy k and its dissipation ε, the zero-gradient inlet boundary condition resulted in k values of the order of 2 x 10^{-5} m^2/s^2 near the centre and over 0.001 m^2/s^2 near the walls of the tunnel. Rough wall boundary conditions were imposed to all solid surfaces, with a small roughness length of z_0 = 0.001 m.

The source emitted clean helium. The boundary conditions of the emitting area were 'given value and no diffusion' for all variables except k and ε, for which zero-gradient was chosen, based on previous experience [21], in order not to suspend the turbulence that would be produced due to the high speeds and the sharp corners of the source geometry. The maximum CFL number of the whole domain was limited to 6. Due to the small grid size and the very high speeds, the simulation time steps were very low (initial stabilized step of about 5 x 10^{-5} s). The total wall-clock time for the simulation of test 12 to reach 200 s, was about fifteen days, using MPI parallelization at 20 CPU cores.

Figure 4 presents part of the simulated geometry and of the sensors. The tunnel inclination is from left (low altitude) to right (high altitude). The wind direction is from right to left for both tests and thus the wind acts against the buoyancy. Sensors 3, 5, 6, 7, 11, 12, 13, 18, 20, with the red colour, were at the same positions during all the tests. The orange sensors, with the suffix "u", were available only at the upwards release (test 3), while the pink ones, with the suffix "d" only at the downwards one (test 12).

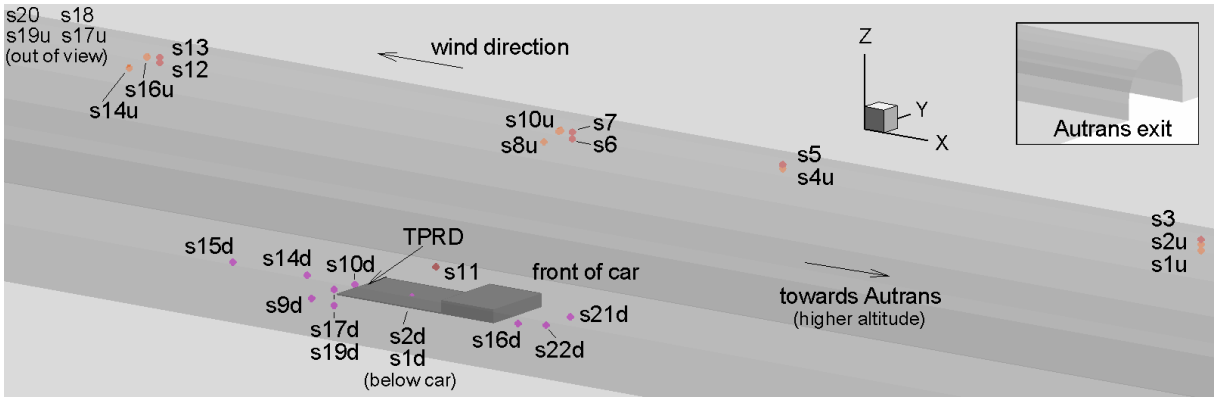

Figure 4. An about 35m long part of the tunnel, where the car and most of the sensors can be seen. At the inset the Autrans exit is shown, in order to make clearer the horseshoe shape of the tunnel

The coordinates of the sensors, in meters, can be seen at Table 1; the values are rounded for readability reasons. It is noted that along the actual tunnel the height varied slightly, while at the simulations it is constant. In order to account for that, the CFD sensors that are close to the ceiling have the same distance from the ceiling (and not from the street) with the experimental ones. Regarding the sensors

that are close to the street, the 1 cm high obstacle discussed earlier should be taken into account. Thus for example the distance of sensor 16d from the street is 2 cm (while its CFD Z-coordinate is 3 cm).

Table 1. Approximate positions of the experimental sensors in the CFD coordinate system.

		S1u	**S2u**	**S3**	**S4u**	**S5**	**S6**	**S7**	***S8u***	***S9u***	**S10u**	**S11**	**S12**	**S13**	***S14u***	***S15u***	**S16u**	**S17u**	**S18**	**S19u**	**S20**	–	–
upwards	X	23.9	23.9	23.9	11.9	11.9	5.92	5.92	5.92	5.92	5.92	2.01	-5.92	-5.92	-5.92	–	-5.92	-11.9	-11.9	-23.9	-23.9	–	–
	Y	0.00	0.00	0.00	0.00	0.00	0.00	0.00	-1.12	-0.46	-0.54	0.00	0.00	0.00	-1.20	–	-0.50	0.00	0.00	0.00	0.00	–	–
	Z	4.72	4.86	4.98	4.87	4.97	4.67	4.83	4.83	4.96	4.96	1.03	4.71	4.83	4.83	–	4.96	4.89	5.06	4.87	5.01	–	–
		S1d	**S2d**	**S3**	***S4d***	**S5**	**S6**	**S7**	***S8d***	**S9d**	**S10d**	**S11**	**S12**	**S13**	**S14d**	**S15d**	**S16d**	**S17d**	**S18**	**S19d**	**S20**	**S21d**	**S22d**
downw.	X	1.32	1.32	23.9	–	11.9	5.92	5.92	–	0.00	-0.32	2.01	-5.92	-5.92	-1.69	-3.82	4.37	-0.07	-11.9	-0.07	-23.9	5.86	5.86
	Y	0.00	0.00	0.00	–	0.00	0.00	0.00	–	-2.14	0.00	0.00	0.00	0.00	0.00	0.00	0.00	-1.16	0.00	-1.16	0.00	0.00	-0.95
	Z	0.03	0.20	4.98	–	4.97	4.67	4.83	–	0.41	0.25	1.02	4.71	4.83	0.27	0.26	0.03	0.41	5.06	0.03	5.01	0.41	0.41

Because at the simulations, due to symmetry, the domain includes only negative Y-axis values, the experimental sensors that are at positive axis are transferred at the symmetrical position at negative axis (sensors with italics at Table 1). In case that position is very close to another sensor, the sensor is ignored at CFD (grey sensors). Underlined sensors have the same positions at both tests. At CFD more sensors exist, that were not present at the experiment, but in general they will not be discussed here.

4.0 RESULTS AND DISCUSSION

4.1 Downwards release

An overview of the general flow and dispersion characteristics in case of downwards hydrogen release from a car inside an inclined tunnel, is presented in a previous work [4]. Also, details about the possible flow patterns during the early stages of a release below a car can be found at [21]. In short, the high-speed jet impinges on the street and spreads horizontally with a speed of many dozens meters per second, usually forming a hydrogen sheet that gets out of the limits of the car (unless if the flow rate is very small) from its back in its sides. Hydrogen accumulates at the limits of this sheet not very far from the car and is transferred upwards, due to buoyancy, in the form of blister-like structures. After some time those structures partly merge and surround the car. Hydrogen impinges on the ceiling with a speed of few meters per second and spreads towards both sides of the tunnel. The presence of low ventilation, results in asymmetric spreading along the ceiling. Higher ventilation transfers the hydrogen cloud downwind. As the time passes hydrogen accumulates at the ceiling and the inclination plays an increasing role. During the release, the ceiling impingement results in a kind of hydrogen gap there. After the end of the release hydrogen resettles and also covers that gap.

Figure 5 presents some of the results of the current CFD simulation of experimental test 12, with downwards helium release. At Figure 5a a helium isosurface with volume concentration equal to 2.1% is shown, with orange colour, surrounding the right part of the vehicle, which is with grey colour. Also the concentration contours at the symmetry plane (Y=0) are presented, for the time of 30 s (Figure 5a) and 60 s (Figure 5b) after the beginning of the release.

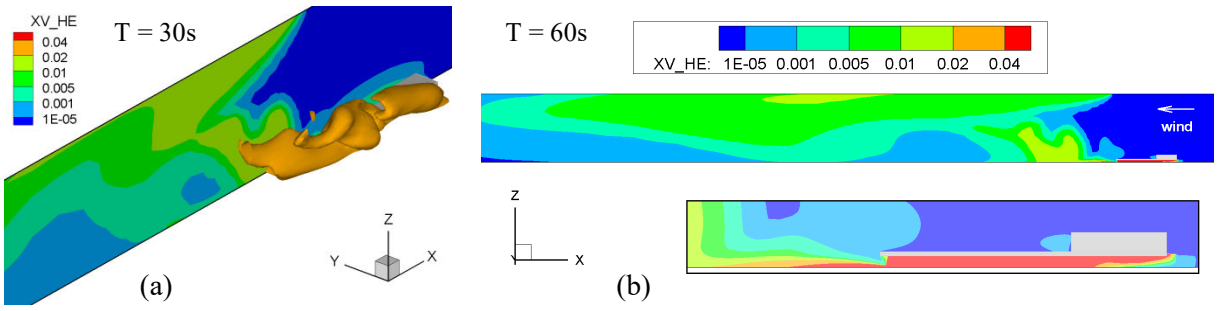

Figure 5. (a) Helium volume concentration contours and the 0.021 isosurface at the time of 30 s. (b) Concentration contours at 60 s. The inset zooms in the area around the vehicle

The orange isosurface of Figure 5a is formed from three individual elongated (due to the wind) blister-like structures. Helium is transferred mainly through those unsteady structures and this creates an uneven and stochastic gas distribution around the car. This should be taken into account when comparing CFD results with experimental data close to the vehicle. The two structures of Figure 5a at the back and at the sides of the car are believed to be partly created due to the 'fresh air entrainment' effect, which is explained at [21] and was clearly identified in this study also. In short, due to the jet and the severe horizontal spreading of helium close to the street, fresh air enters from the back of the car just below the chassis towards the jet source. One of the results of this effect can be seen for example at the inset of Figure 5b, where at the right side of the jet concentrations are much higher compared to the left side (step at the red contour), due to the fresh air that has entered from behind.

Helium is transferred towards the ceiling mainly through the structure at the back of the car (Figure 5a), forming a wide area with concentrations above 1% at 30 s. The other structure at the sides of the vehicle has a twistering, screw-like shape, which is common in such cases, when ventilation is present. Through this structure helium is transferred towards the top part of the sides of the tunnel and at the ceiling also. The third structure, at the front, has a "C" shape, similar to that of the front structures of [21]. Of course we do not know if the particular structures were present at the experiment, but it is important to know that some kind of (similar or not) structures were probably formed.

Concerning the comparison with the experiments, it would be good to know if similar physical phenomena occur (or may occur) at both the simulations and in reality. From Figure 5 it is clear that helium is not transferred upwind, i.e. there was no backlayering for the specific wind speed and also no helium propagates in front of the car. Indeed, at both the experiments and the CFD, sensors 3, 5, 6, 7, 21d and 22d have zero values. Regarding the spreading of helium along the ceiling we can see that at 60 s most of the cloud is transferred downwind. Also the concentrations have dropped below 1% at almost all ceiling length. It is noted that by 60 s the source strength is only the 26.6% of the initial one.

A comparison of the values of the sensors between experiment and CFD is more meaningful at the ceiling sensors, where the measurements are more independent from stochastic parameters. Figure 6 presents such a comparison for all the ceiling sensors with values different than zero.

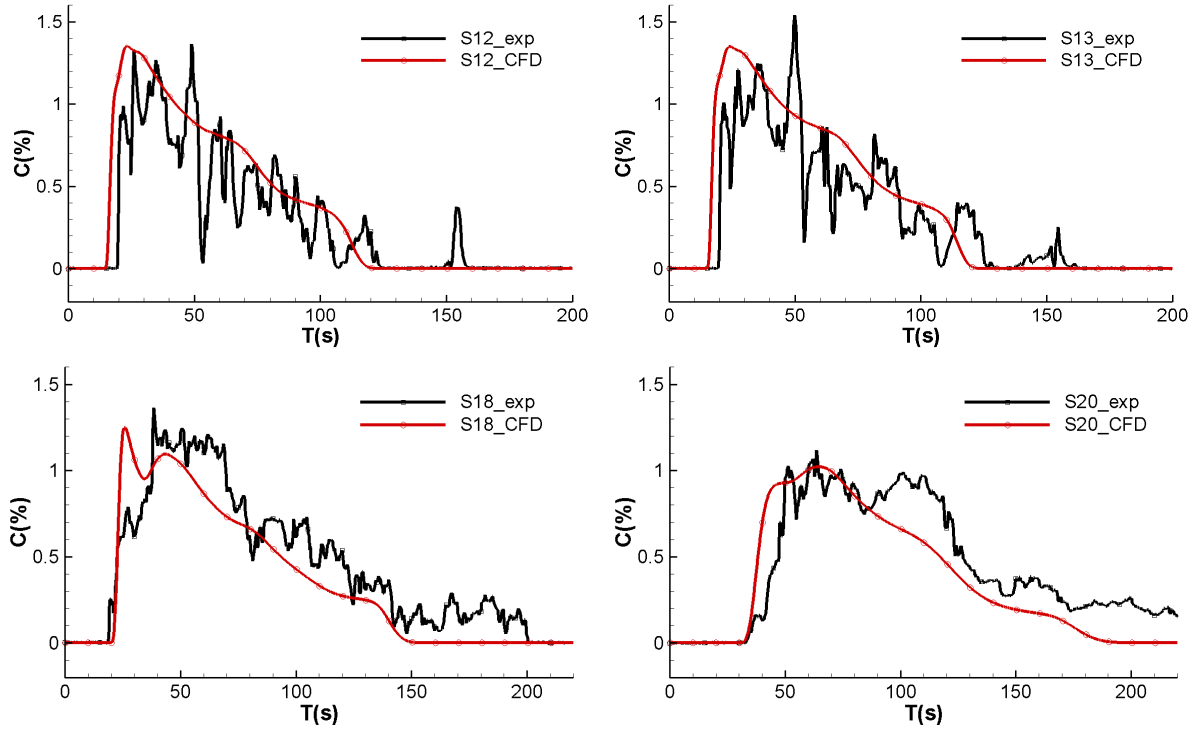

Figure 6. Comparison of experimental and CFD volume concentrations' timeseries at ceiling sensors

The general conclusion from Figure 6 is that a very close agreement between experimental and CFD values exists. The arrival times, the concentration maximums and the time they occur and the rate the concentrations drop are more or less the same, given the uncertainties of both the experiment and the CFD. On the other hand, there is a tendency of CFD to provide all the values slightly faster, especially at the more distant sensors 18 and 20. Additionally, the CFD values become zero earlier in all sensors. This has mainly to do with the wind velocity, as it was concluded with several CFD sensitivity tests that were performed. At CFD the bulk velocity was the same with the average measured value. This results in a higher velocity than the experimental one at the measurement point, due to the developed velocity profile. Simulation tests with slightly lower velocity ameliorated the results. It is noticed that at as we go away from the source, at 6 m, 12 m and 24 m, in general the arrival times increase (20 s, 22 s and 40 s respectively), the peak values decrease (1.4%, 1.3% and 1.1%) and the signal durations increase (110 s, 180 s and 280 s).

Figure 7 presents the timeseries of experimental sensors 8d and 9d, which are at symmetric points and should ideally have the same values (at the simulations they are both represented with one sensor). We see though that the signals are stochastic and present differences. This is not a problem of the measurements, but a characteristic of the unsteady nature of the flow close to the car. At test 3, where there were also symmetric sensors close to the ceiling, their measurements were very close.

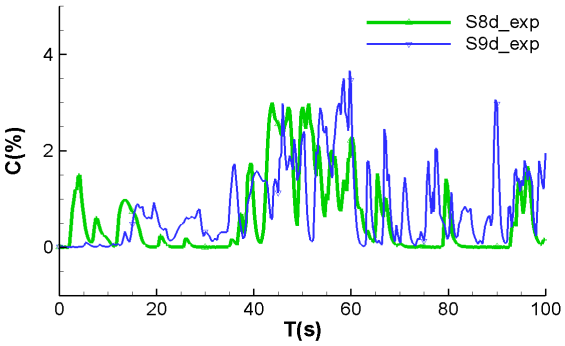

Figure 7. Experimental volume concentrations at two symmetric sensors, namely 8d and 9d

Based on the previous discussion, at the sensors around the car several differences between CFD and experiment can be expected. It is useful to present their values though, in order to try to draw some conclusions. At Figure 8 the concentration timeseries at Y=0, at 3.67 m, 1.54 m and 0.17 m behind the car, at about 26 cm from the ground are presented.

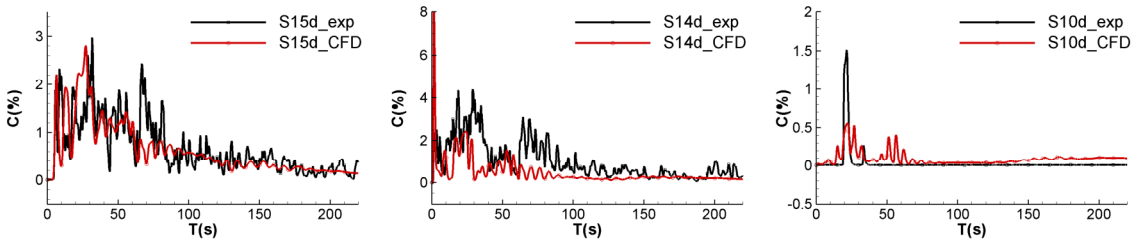

Figure 8. Experimental and CFD volume concentrations' timeseries at the sensors behind the vehicle

At the most distant sensor 15d, the values are in very good agreement. This is a sign that the backwards extend and strength of the helium cloud/ blister (see Figure 5) is similar between CFD and experiment. At sensor 14d, during most of the time CFD underestimates the concentrations. Examination of the CFD results (not presented here) showed that helium arrives at that sensor mainly sidewards. The same happens for sensor 11 (not presented here), where again CFD underestimates. It is thus believed that the lateral cloud extension and recirculations might not be modelled perfectly from CFD, possibly due to the inaccuracies of simulating a high-speed impinging jet. Sensor 10d is at

a point that is influenced both from the fresh air entrainment effect and from the wind. This is why its signals are weak, making any comparison risky. Its maximum at both CFD and experiment occurs at about 22 s.

At Figure 9 the values of the side sensors 9d and 19d are presented, along with 1d and 2d that are below the car. Examination of the CFD results (not presented here) shows that sensor 9d is in general at a position very close to blister-like structures/ helium clouds. Most of the time it is just outside them and this explains the underprediction shown at Figure 9. During the first five seconds though, sensor 9d is at a 'nose' of such a structure and this results at the early CFD peak. A position of the sensor 20 cm towards the back would result in 10 times lower values during the first seconds. Thus the specific position is tricky and any discrepancy may be due to 'random' reasons. Sensor 19d is close to the street level, inside the horizontal helium sheet. CFD values compare very well with the experimental ones, except of the first seconds, when there is an overprediction. Those early peaks also appear at the sensors 1d and 2d below the car and generally in all sensors of Figure 9. It should be noted here that at CFD the release starts abruptly, while at the experiment there was a valve that opened gradually during a period of 0.7 s. Other possible explanations of the early CFD peaks are the inaccuracies of the turbulence levels and structure below the car and of the Birch approach during the first seconds.

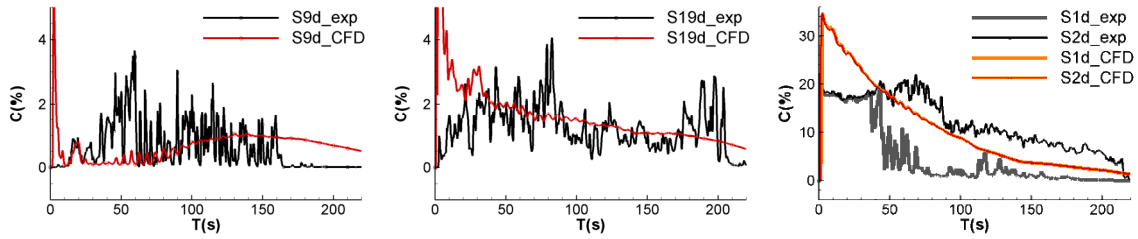

Figure 9. Experimental and CFD volume concentrations at the sides and below the vehicle

It is interesting to comment on the two sensors below the car, at the right of Figure 9. We notice that at the experiment the two sensors measure the same values, around 18%, till the time of 37 s and then the values of sensor 1d, which is closer to the street, drop abruptly to about 1% and stay there. This is believed to be due to another phenomenon that is described in [21], the street-level air entrainment from the front of the car. As the time passes and the buoyancy starts playing a role below the car, fresh air enters from the street level at the front of the car, creating a backflow (see also Figure 5b). This flow gets stronger and is transferred towards the jet, till it collides with the jet recirculation. It is believed that at about 37 s sensor 1d got into the region of this flow. At CFD that region is smaller.

4.2 Upwards release

Having validated the ADREA-HF CFD code against the experimental case of downwards release in a real, sloped tunnel with natural ventilation (test 12), it was attempted to investigate whether CFD could help understand, at least partly, the 'strange' behaviour of helium cloud in the case of experimental test 3. The particular test represents a rare case where there seems to be some kind of balance between the buoyant forces and the low-speed natural ventilation which acts against the buoyancy. Normally the concentrations at the ceiling sensors increase rapidly to a peak value and then drop smoothly, as in Figure 6. At the experimental test 3 though, the peak values are kept for many dozens of seconds, creating a 'plateau'. At the most distant downwind sensors (s19u, s20) the concentrations are kept close to their maximum values for hundreds of seconds, throughout the test. Also, at most sensors a sudden increase of concentrations ('step') appears after the end of the release, which also needs an explanation.

Figure 10 presents the CFD concentration contours for 20 s and 60 s. Helium propagates towards both sides, but due to the wind the upwind cloud is thicker, while the downwind one is longer, having higher longitudinal propagation speed. Ceiling concentrations are in general above 1%. The jet axis is slightly tilted and at 20 s it hits the ceiling at X= -0.37 m, with an angle of 9 degrees.

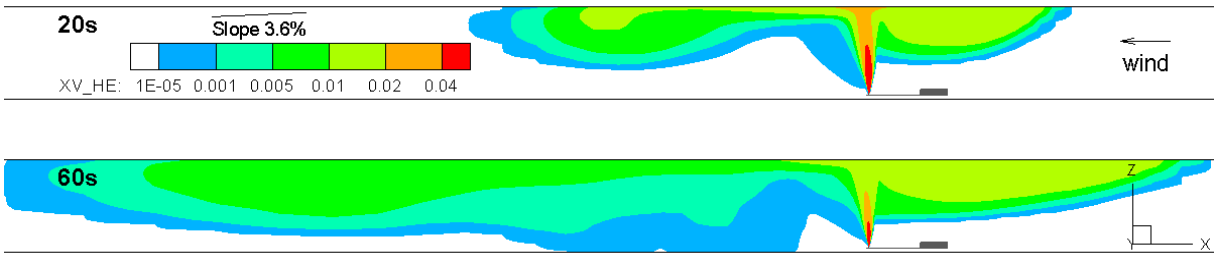

Figure 10. CFD helium volume concentration contours at Y=0 for test 3 at 20 s and 60 s

The concentrations of three sensors of the Y=0 plane are shown in Figure 11. They are at about 0.3 m from the ceiling and at X coordinates of -6 m, 6 m and 24 m (s13, s7 and s2u respectively).

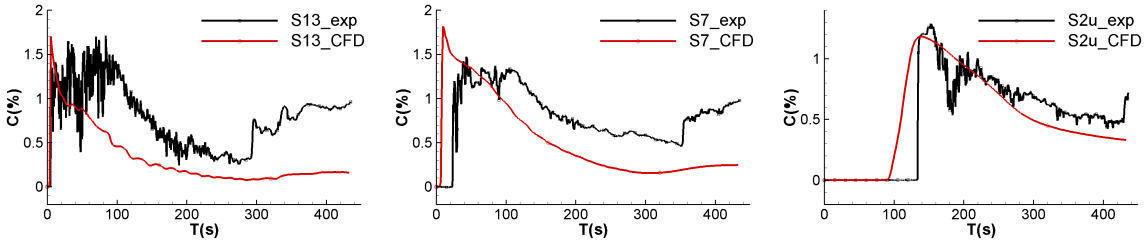

Figure 11. Experimental and CFD volume concentrations' timeseries at ceiling sensors for test 3

We can see that the peak values of CFD and experiment are of the same order. Also the rate the concentrations drop is more of less the same, even if at CFD the values start dropping earlier (this discrepancy is bigger at sensors 17u and 19u, at -12 m and -24 m, not shown here). Additionally, neither the 'plateau' of the first 100 s of s7 and s13, nor the 'step' that appears at the three sensors after the end of the release are predicted from CFD, which means that some aspects of the experimental flow field were not reproduced. It would be interesting to try to understand what had happened at the experiment though.

Several CFD sensitivity tests were performed in order to try to elucidate the experimental results. It was found that the 'steps' were most probably due to helium displacement at the ceiling. At CFD simulations that presented 'steps' at the concentrations' time series, the mechanism of their creation was as follows: as the source flow rate decreased, when the helium jet was weak enough, the horizontal velocities after the ceiling impingement were very low and thus the high-concentrations' (very close to the ceiling) helium that had gathered downwind (at X< -6 m) started moving towards the Autrans exit (right side of Figure 10) due to the buoyancy and to the slope of the tunnel. That thin moving cloud passed consecutively from sensors 13, 7, 4, 2u. Indeed, from the experiments the 'steps' at the specific sensors appear at 290 s, 350 s, 390 s and 420 s respectively, which corresponds to a cloud moving towards the Autrans exit. It is interesting that below this thin helium-rich slowly moving cloud, the lower-concentrations' helium layers were slowly moving towards the opposite direction (i.e. as the wind blew) and their concentrations slowly decreased, as helium was transferred downwind. Thus the (very low) wind just 'eroded' the helium layers from below (and did not massively transfer them) and this mechanism might be also playing a role in the interpretation of the 'plateau' mentioned earlier and in the very slow decrease of the concentrations at sensors 19u and 20.

Even if the physical mechanisms described at the previous paragraph partly explain the 'strange' experimental results, the CFD simulations that revealed those mechanisms had very low helium jet speed at the source, something which is difficult to justify. Also, except of the existence of the 'steps', their results so far were not good. It is noted that the experimental timeseries of s13 and s7 (Figure 11), which are at the same horizontal distance from the source (at X= -6 m and 6 m), provide some evidence that helium reached the ceiling at a point much closer to s13 than to s7, since s13 presents a more turbulent signal with much shorter arrival time (4.3 s instead of 23 s). One possible explanation

for this is that the jet speed had indeed relatively low values, at least when arriving at the ceiling. At the main CFD simulation (Figures 10, 11), the ceiling impingement velocity was high though and thus the downwind-oriented helium escaped and never came back. Several parameters were changed at additional CFD simulations (like the geometrical representation of the front of the car, the inclusion of the experimental masts, the geometry of the ceiling, the turbulence intensity at the entrance of the tunnel, the roughness length, the wind velocity) in order to see whether each one of them could affect the jet or other important factors of the flow field, but they had a relatively minor influence on the results and certainly not towards creating some kind of 'plateau' or 'step' at any of the sensors.

It is true that not all issues regarding the experimental results and the CFD simulations of test 3 are clarified and there are still unanswered questions that need further investigation. If during the campaign some sensors existed at positions away from the others (for example at intermediate heights, or at long distances), it might be easier to interpret the experimental measurements of the ceiling sensors. Also it would be good to have a representation of the flow field, for example with velocity measurements at more points, but that would have increased the experimental efforts. Regarding the CFD, more research is needed, maybe with a focus on the source and the validity of the Birch approach. In any case, test 3 of CEA experiments seems to be a tricky and special case, with inherent difficulties regarding the full explanation of its results. Until the relevant knowledge gaps are filled, it might not be a good choice for CFD validation, especially without taking into account its particularity.

5.0 CONLCUSIONS

The main conclusion of this work is that the ADREA-HF code presented good predictive capabilities of the experimental results and can thus be used in safety studies of hydrogen dispersion inside tunnels, including ventilated and sloped ones. It was also made clear that CFD can help in the interpretation of experimental facts, even in the cases the results are not accurately reproduced. CFD is a strong tool that can also contribute to the design of the experiments and in parametric studies. On the other hand, some limitations of CFD were identified, like the always necessary simplifications of the examined problem and the accuracy of the parameterizations used. Concerning the experiments, it was made clear that it is good to try to have a general, even approximate, overview of the whole flow field and not to focus only at the areas of interest. For future work it would be helpful to examine more CEA experiments, especially because of the statistical nature of the results. For CFD validation it would be even better to have reduced-scale experiments, under more controllable conditions.

6.0 ACKNOWLEDGMENTS

Part of this research was funded from the Clean Hydrogen Joint Undertaking through grant agreement No 826193 (project HyTunnel-CS). The Joint Undertaking receives support from the European Union's Horizon 2020 research and innovation programme. This work was also supported by computational time granted from the National Infrastructures for Research and Technology S.A. (GRNET) in the National HPC facility - ARIS - under project ID pr014025 (H2TUN).

REFERENCES

1. Abánades, A., Perspectives on Hydrogen, *Energies*, **16**, 2022, 437.
2. IEA, Global EV Outlook 2022, Paris, https://www.iea.org/reports/global-ev-outlook-2022.
3. Giannissi, S.G., Venetsanos, A.G., Rattigan, W. and Lyons, K., CFD Dispersion Simulations of Compressed Hydrogen Releases Through TPRD Inside Scaled Tunnel, 10th International Conference on Hydrogen Safety (ICHS2023), 19-21 September 2023, Québec City, Canada, paper ID151.
4. Koutsourakis, N., Tolias, I.C., Giannissi, S.G. and Venetsanos, A.G., Numerical Study of the Effects of Tunnel Inclination and Ventilation on the Dispersion of Hydrogen Released from a Car, Proceedings of the 9th International Conference on Hydrogen Safety (ICHS2021), 21-23 September 2021, Edinburgh, United Kingdom, pp. 1641-1652.

5. Venetsanos, A.G., Papanikolaou, E.A. and Bartzis, J.G., The ADREA-HF CFD Code for Consequence Assessment of Hydrogen Applications, *International Journal of Hydrogen Energy*, **35**, No. 8, 2010, pp. 3908-3918.
6. Zhao, S., Li, Y.Z., Kumm, M., Ingason, H. and Liu, F., Re-direction of smoke flow in inclined tunnel fires, *Tunnelling and Underground Space Technology*, **86**, 2019, pp. 113-127.
7. Venetsanos, A., Huld, T., Adams, P. and Bartzis, J., Source, Dispersion and Combustion Modelling of an Accidental Release of Hydrogen in an Urban Environment, *Journal of Hazardous Materials*, **105**, 2003, pp. 1-25.
8. Huang, T., Zhao, M., Ba, Q., Christopher, D.M. and Li, X., Modeling of Hydrogen Dispersion from Hydrogen Fuel Cell Vehicles in an Underground Parking Garage. *International Journal of Hydrogen Energy*, **47**, 2022, pp. 686-696.
9. Middha, P. and Hansen, O.R., CFD Simulation Study to Investigate the Risk from Hydrogen Vehicles in Tunnels. *International Journal of Hydrogen Energy*, **34**, 2009, pp. 5875-5886.
10. Breitung, W., Bielert, U., Necker, G., Veser, A., Wetzel, F.J. and Pehr, K., Numerical Simulation and Safety Evaluation of Tunnel Accidents with a Hydrogen Powered Vehicle, Proceedings of the 13th World Hydrogen Energy Conference, 12-15 June 2000, Beijing, China, pp. 1175-1181.
11. Mukai, S., Suzuki, J., Mitsuishi, H., Oyakawa, K. and Watanabe, S., CFD Simulation of Diffusion of Hydrogen Leakage Caused by Fuel Cell Vehicle Accident in Tunnel, Underground Parking Lot and Multi-Story Parking Garage, Proceedings of the 19th International Technical Conference on the Enhanced Safety of Vehicles (ESV), 6-9 June 2005, Washington D.C., U.S.A., paper No.05-0293.
12. Houf, W.G., Evans, G.H., Merilo, E., Groethe, M. and James, S.C., Releases from Hydrogen Fuel-Cell Vehicles in Tunnels. *International Journal of Hydrogen Energy*, **37**, 2012, pp. 715-719.
13. Bie, H.Y. and Hao, Z.R., Simulation Analysis on the Risk of Hydrogen Releases and Combustion in Subsea Tunnels, *International Journal of Hydrogen Energy*, **42**, 2017, pp. 7617-7624.
14. Hansen, O.R., Hansen, E.S., Kjellander, M.T. and Martini, R., CFD Study to Assess Safety Aspects of TPRD Releases from Heavy-Duty Hydrogen Vehicles and Trains in Tunnels. *Chemical Engineering Transactions*, **90**, 2022, pp. 91-96.
15. He, J., Kokgil, E., Wang, L. and Ng, H. D., Assessment of Similarity Relations using Helium for Prediction of Hydrogen Dispersion and Safety in an Enclosure, *International Journal of Hydrogen Energy*, **41**, No. 34, 2016, pp. 15388-15398.
16. Bouix, D., Sauzedde, F., Manicardi, P., Martin, M., Forero, D., Studer, E., Bernard-Michel, G., Koudriakov, S. and Gueguen, H., Full-Scale Tunnel Experiments for Fuel Cell Hydrogen Vehicles: Gas Dispersion, Proceedings of the 9th International Conference on Hydrogen Safety (ICHS2021), 21-23 September 2021, Edinburgh, United Kingdom, pp. 1211-1223.
17. Melin, C., Studer, E., Forero, D., Bernard-Michel, G., Bouix, D. and Sauzedde, F., Hydrogen Dispersion in a Full-Scale Road Tunnel: Experimental Results and CFD Analysis, 10th International Conference on Hydrogen Safety (ICHS2023), 19-21 September 2023, Québec City, Canada, paper ID127.
18. Bartzis, J.G., ADREA-HF: A Three-Dimensional Finite Volume Code for Vapour Cloud Dispersion in Complex Terrain, Report EUR 13580 EN, 1991.
19. Waterson, N.P. and Deconinck, H., Design Principles for Bounded Higher-Order Convection Schemes – a Unified Approach, *Journal of Computational Physics*, **224**, 2007, pp. 182-207.
20. Tolias, I.C. and Venetsanos, A.G., Comparison of Convective Schemes in Hydrogen Impinging Jet CFD simulation, 6th International Conference on Hydrogen Safety, 19-21 October 2015, Yokohama, Japan, paper ID251.
21. Koutsourakis, N., Tolias, I.C., Giannissi, S.G. and Venetsanos, A.G., Numerical Investigation of Hydrogen Jet Dispersion Below and Around a Car in a Tunnel, *Energies*, submitted 2023.
22. Birch, A.D., Brown, D.R., Dodson, M.G. and Swaffield, F., The Structure and Concentration Decay of High Pressure Jets of Natural Gas, *Combustion Science and Technology*, **36**, Nos. 5-6, 1984, pp. 249-261.